journal of the mechanical behavior of biomedical materials 156 (2024) 106598

Contents lists available at ScienceDirect

Journal of the Mechanical Behavior of Biomedical Materials

journal homepage: www.elsevier.com/locate/jmbbm

Post-printing processing and aging effects on Polyjet materials intended for the fabrication of advanced surgical simulators

Nicolas Emiliani [a], Rita Porcaro [b], Gregorio Pisaneschi [c], Barbara Bortolani [a], Fabrizio Ferretti [a], Francesco Fontana [c], Giampaolo Campana [c], Maurizio Fiorini [b], Emanuela Marcelli [a], Laura Cercenelli [a,*]

[a] eDIMES Lab - Laboratory of Bioengineering, Department of Medical and Surgical Sciences (DIMEC), Alma Mater Studiorum University of Bologna, 40138, Bologna, Italy
[b] Department of Civil, Chemical, Environmental and Materials Engineering (DICAM), University of Bologna, Via Terracini 28, 40131, Bologna, Italy
[c] Department of Industrial Engineering (DIN), University of Bologna, Viale del Risorgimento, 40136, Bologna, Italy

ARTICLE INFO

Keywords:
3d printing
Polyjet technology
Surgical simulation
Biomaterials
Mechanical testing

ABSTRACT

Material Jetting (MJ) 3D printing technology is promising for the fabrication of highly realistic surgical simulators, however, the changes in the mechanical properties of MJ materials after post-printing treatments and over time remain quite unknown.

In this study, we investigate the effect of different post-printing processes and aging on the mechanical properties of a white opaque and rigid MJ photopolymer, a white flexible MJ photopolymer and on a combination of them. Tensile and Shore hardness tests were conducted on homogeneous 3D-printed specimens: two different post-printing procedures for support removal (dry and water) and further surface treatment (with glycerol solution) were compared. The specimens were tested within 48 h from printing and after aging (30–180 days) in a controlled environment.

All groups of specimens treated with different post-printing processes (dry, water, glycerol) exhibited a statistically significant difference in mechanical properties (i.e. elongation at break, elastic modulus, ultimate tensile strength). Particularly, the treatment with glycerol makes the flexible photopolymer more rigid, but then with aging the initial elongation of the material tends to be restored. For the rigid photopolymer, an increase in deformability was observed as a major effect of aging. The hardness tests on the printed specimens highlighted a significant overestimation of the Shore values declared by the manufacturer. The study findings are useful for guiding the material selection and post-printing processing techniques to manufacture realistic and durable models for surgical training.

1. Introduction

The emergence of additive manufacturing (AM), more commonly known as 3D printing, has transformed traditional manufacturing processes and revolutionized product development across various fields, including medicine (Sun et al., 2023), (Aimar et al., 2019), (Vaz and Kumar, 2021). Unlike subtractive manufacturing techniques that involve removing material from a larger block, AM adopts the innovative approach of building up objects layer by layer, which allows for the creation of highly complex and customized geometries. The Material Jetting (MJ) process, also known as Polyjet 3D printing (Stratasys Ltd., Rehovot, Israel), is a technology based on the combination of inkjet and photo-polymerization. The materials are simultaneously jetted drop by drop in a layer-wise build procedure. The layered structure is achieved by a precise lowering of the build platform, while the printing block continues creating the layers. Each applied polymer layer is cured immediately by means of an ultraviolet light source, which is located on the side of the printing block. Where overhangs or complex shapes require support, the Polyjet 3D printer jets a removable support material. To ensure an even surface finish for the following layers, each applied layer is smoothed by means of a roller, located in the printing block.

The Polyjet 3D printing technology allows the fabrication of multi-material structures with a resolution of up to 16 μm and the

* Corresponding author.
E-mail address: laura.cercenelli@unibo.it (L. Cercenelli).

https://doi.org/10.1016/j.jmbbm.2024.106598
Received 15 March 2024; Received in revised form 6 May 2024; Accepted 23 May 2024
Available online 24 May 2024

simultaneous use of up to six different materials in the printer. By using different nozzles, it is possible to locally mix rubber-like materials with rigid ones in order to obtain parts with variable hardness ranging from Shore A30 to A95. The results of this versatility are the so-called Digital Materials (DMs) that may have customizable mechanical properties. Usually, the printed model is completely embedded in the support material, including the topmost surfaces to ensure evenness ("matte" surface finish). The user can also choose a "glossy" finish (i.e. not to cover the topmost model surfaces with the support material).

The high resolution and the possibility to print multiple materials all in a single build, and with customizable mechanical properties make Polyjet technology ideal for the application in many sectors such as automotive, architecture, consumer goods, for the fabrication of highly realistic and multi-material prototypes, aesthetic components with precise and smooth surfaces, functional parts such as tooling, jigs and fixtures, and master molds for over-molding.

In the healthcare sector, they are also particularly interesting and promising for medical education and surgical training where it is very important to reproduce simulators with materials that give the most realistic tactile feedback so that the learners can improve their skills in highly realistic conditions. Depending on the needs, several materials (colour, properties, textures) may be required to create a proper phantom for surgical simulation, and many experiences of using multi-material jetting technology (like Polyjet) for these purposes can be found in the literature (Valls-Esteve et al., 2023).

In the field of ear-nose-throat (ENT) surgery, patient-specific 3D printed multimaterial sinus models for training in endoscopic sinus surgery have been developed and validated by residents and experts (Molinari et al., 2022), (Suzuki et al., 2022). Additionally, 3D-printed models have been widely employed for training in endoscopic skull base surgery (Langdon et al., 2023).

In the field of urology, Wake et al. (2016) 3D printed a cancerous patient-specific kidney model with accurate anatomy for applications in urological oncology using a transparent flexible material as the main cortex and the Polyjet rigid photopolymers in different colours as the remaining structures. Kusaka et al. (2015) also 3D printed a kidney graft and pelvic cavity model via the PolyJet printing process using mainly flexible photopolymers with different colours, and the model was successfully applied for accurate simulation of the surgical procedure of kidney transplantation. Komai et al. (2016) also fabricated a patient-specific, full-scale kidney model via the PolyJet process, which included a removable tumor combined with its margin, which provided the surgeons with tactile sensation and aided in effectively determining the incision line and angle for tumor resection.

For cardiac applications, Yoo et al. (2017) fabricated cardiac models with congenital heart disease using flexible photopolymers via the PolyJet process, and the models were used by trainees for performing the required surgical procedures. In another example, Kiraly et al. (2016) printed via the PolyJet process a scaled-up flexible, hollow heart model with a congenital defect that was used for preoperative rehearsal. Furthermore, Yang et al. (2015) printed a heart model using flexible photopolymers with different colours to distinguish different parts in the heart model that could also be disassembled for surgical practice, such as a rehearsal of extended septal myectomies. Other experiences of 3D printing of heart models for mitral valve interventions can be found in the review by Bharucha et al. (2023).

In the hepatology field, Zein et al. (2013) created 3D-printed liver models from living donors and their recipients using the PolyJet process. The liver models were useful for the comprehension of the spatial relationship between the vascular and biliary anatomies, and for enabling hands-on surgical planning and training. Souzaki et al. (2015) also 3D printed a model of a patient's liver with a tumor using the PolyJet process. The model was used for viewing the anatomies and the relative positions of the portal vein, hepatic vein, and tumor, as well as to determine the resection line for removing the tumor.

For neurological applications, Erbano et al. (2013) fabricated 3D intracranial aneurysm models using rigid photosensitive liquid resins, via the PolyJet process. The models replicated the accurate size, shape, and location of the intracranial aneurysms, although were not useful for clipping and dissecting exercises due to the rigid nature of the material. Khan et al. (2014) created a hollow cerebral aneurysm and vasculature physical model by using PolyJet printing process and flexible photopolymers. These models were used for neurosurgical trainees for better anatomical understanding, as well as for the determination of proper surgical approaches and tools. Similarly, Wurm et al. (2011) used the PolyJet process to 3D print an aneurysm model, which was used as a reusable part for several clipping exercises in microsurgical simulation.

In the pulmonology field, Kurenov et al. (2015) 3D printed models of human pulmonary arteries using the PolyJet process and flexible photopolymers. The models were accurate for clinical purposes and were used to design a catheter for regional lung chemotherapy. Furthermore, Bustamante et al. (2014) fabricated 3D-printed tracheobronchial tree models using the PolyJet process to aid medical professionals in improving familiarity with endoscopic bronchial anatomy. The models were examined with a flexible fiberoptic bronchoscope and the obtained images were similar to the actual views of the organ during lung isolation.

In the above context, the assessment of the mechanical properties of the 3D-printed parts of the simulators is crucial. The properties of Polyjet materials are not provided in detail by the manufacturer, and the influencing factors such as the material jetting process (e.g., the anisotropy due to layer-wise build procedure) or the post-printing treatments are not taken into account or poorly investigated (Tyagi et al., 2022).

Some studies have been conducted to evaluate the impact of printing process parameters on the dimensional accuracy of the printed parts (Yap et al., 2017), (Cheng and Huang, 2020), (Tee et al., 2020), (Khoshkhoo et al., 2018), (Königshofer et al., 2021) and on the mechanical properties of various Polyjet materials (Dizon et al., 2018). Stiffness and fracture stress are significantly affected by part orientation during printing (Königshofer et al., 2021), (Cazón et al., 2014), (Stansbury and Idacavage, 2016), (Bass et al., 2016), (Hong et al., 2018). Part spacing along the Y-axis has the highest effect on the relaxation modulus (Gay et al., 2015). Some studies evaluated the effect of surface finish and printing modality on the mechanical properties of Polyjet 3D printed parts (Pugalendhi et al., 2020), (Grimaldo Ruiz et al., 2022), (Mueller et al., 2015), (Blanco et al., 2014). It was observed that the finishing operations had no effect on the tensile strength of the 3D-printed parts, but affected their roughness properties. Also, the glossy surface finish could improve the fatigue life of the Polyjet-printed parts (Moore and Williams, 2015).

In addition to this, the aspects related to the lifetime of the printed parts of a surgical simulator and/or the long-term effect of environmental conditions on them should be considered to assess their expected performance over time (Bochnia, 2023).

Some works have been done to evaluate the changes in the mechanical properties of 3D-printed parts over time. Accelerated aging (weathering test) has been widely employed to study the long-term performance of some printed Polyjet polymers in laboratory settings (Matušú et al., 2021). Weathering protocols involve intense aging of specimens for a short duration to replicate long-term natural degradation. Some previous studies reporting these aging protocols revealed that, for Polyjet rigid materials, the ultimate tensile stress increased and elongation decreased over time, while the modulus of elasticity did not show statistically significant change (Bass et al., 2016), (Vassilopoulos, 2022), (Costa et al., 2013), (Golhin et al., 2023).

To the authors' knowledge, the effect of the post-printing process and aging on the newest Polyjet materials like Agilus30White and its mixture with rigid resins to obtain DMs is poorly investigated.

The purpose of this study is to analyze the mechanical properties of two Polyjet materials of choice for the fabrication of surgical simulators, i.e. Agilus30White and VeroPureWhite, under the effect of different

Table 1
Mechanical properties of the materials used in this study, as taken from the datasheet. * The only available datasheet values are referred to the mixture of Agilus30 Clear/Black and VeroFamily materials.

	Mechanical properties	Test Method	Value
Agilus30White (A)	Tensile Strength	ASTM D-412	2.1–2.6 MPa
	Elongation at Break	ASTM D-412	185–230%
	Shore Hardness	ASTM D-2240	30 - 40 Scale A
VeroPureWhite + Agilus30White (M) *	Tensile Strength	ASTM D-412	3.5–4.5 MPa
	Elongation at Break	ASTM D-412	150–170%
	Shore Hardness	ASTM D-2240	55 - 60 Scale A
VeroPureWhite (R)	Tensile Strength	ASTM D-638-03	50–65 MPa
	Elongation at Break	ASTM D-638-05	10–25%
	Shore Hardness	Scale D	83 - 86 Scale D
	Modulus of Elasticity	ASTM D-638-04	2000–3000 MPa

post-printing treatments and after aging. We evaluated these materials individually and in a mixture corresponding to a Shore A60 value, as set in the GrabCAD print software provided with the printer by the manufacturer.

2. Materials and methods

2.1. Design and fabrication of specimens

Stratasys J720 Polyjet 3D printer was used to fabricate all the specimens of the materials. We tested two raw materials, i.e., the rigid VeroPureWhite (R) and the rubber-like Agilus30White (A). VeroPureWhite is a rigid and opaque photopolymer from the family of Vero, available in seven hues. Particularly, VeroPureWhite contains among the others caprolactone acrylate, acrylic acid 2-hydroxyethyl ester, 2-Propenoic acid, 1,2 ethanediyl ester, 2,6-Bis(1,1-Dymethylethyl)-4-Methyl-Phenol and camphene ('Safety datasheet VeroPureWhite). All materials of the Vero family share similar mechanical, thermal, and electrical properties ('VeroFamily datasheet). Agilus30 is a rubber-like polymer, with superior tear resistance and tensile strength, capable of withstanding repeated flexing and bending cycles ('Agilus30 White datasheet). This material is made from Acrylic acid, 2-hydroxyethyl ester, 2,6 Bis(1,1-Dymethylethyl)-4-Methyl-Phenol, 2-Methoxy-1-methylethyl acetate, 1,7,7-Trimethyltricyclo [2.2.1.02,6] heptane and 4-Methoxyphenol/Mequinol ('Safety datasheet Agilus30 White). Then, a mixture (M) of Agilus30White and VeroPureWhite was set up in order to obtain a DM with an intermediate hardness (Shore A60, FLXA9760-DM), suitable to replicate anatomical structures such as cartilages ('Datasheet Digital Materials). Table 1 shows the mechanical properties of these polymers as reported by the manufacturer. Information about the mass fractions of the material mixtures is not provided by the manufacturer.

Two types of specimens were designed with Fusion360 software (Autodesk Inc, USA): one modified type IA based on ISO 527-4 (Plastics, 2023) with dimensions of 175x20x4mm, intended for the tensile tests; the other based on ISO 48–4:2018 (Rubber and vulcanized or thermoplastic, 2018) with dimensions 50x50x50mm, intended for the Shore hardness tests. The 3D printer is operated with GrabCAD Print software to load the STL (Standard Tessellation Language) files and assign the printing material to each specimen. The specimens were printed as homogenous parts with the orientation of the two major dimensions along XY axes to achieve the optimal strength for the part (Cazón et al., 2014) and with a layer deposition thickness of 27 μm and a matte finish (Fig. 1).

2.2. Post-printing processing and aging conditions

In total, 84 specimens were printed. All the specimens were fabricated with the above-reported printing parameters. Fig. 2 shows the scheme used to divide the specimens into subgroups according to the experimental design of the study.

For the tensile tests, the specimens of the three materials (R, A, M) were divided into two groups according to two different cleaning post-printing procedures: in the first group, the support material was removed in dry conditions (D), while for the other group, a soaking station with water (W) was used to clean the parts. The second differentiation was made based on the possible use of glycerol (G) after the cleaning. Stratasys suggests dipping the printed parts in a 15% glycerol solution for 30 s to strengthen them (Stratasys, 2016). For this reason, a subgroup of the specimens cleaned by waterjet was immersed, once dried, in a 15% glycerol solution (G), while the remaining specimens were simply left to dry without glycerol (nG). For each type of material and each post-printing processing condition, 7 specimens were printed for a total of 42 specimens ($n = 3 \times 2 \times 7$).

For each condition, 5 specimens were mechanically tested within 48 h of printing (T0), with 2 specimens left as spare.

For testing the aging effect (T1), another 42 specimens were 3D-printed, all cleaned with water (W). The specimens were divided into two groups and differed for the use (G) or not (nG) of glycerol solution after the cleaning. To explore the effect of time on the mechanical properties of the cured photopolymers, 7 specimens for each type of material (R, A, M) and each condition (G, nG) were naturally aged for 30 days in a controlled environment ($T = 23 \pm 1.8°C$, $UR = 38 \pm 5\%$) and then mechanically tensile tested (Fig. 3).

For Shore hardness testing, a total of 8 cuboid specimens were 3D-printed, one for each available mixing of Agilus30White and VeroPureWhite, i.e. Shore A 30, 40, 50, 60, 70, 85, and 95. The support material

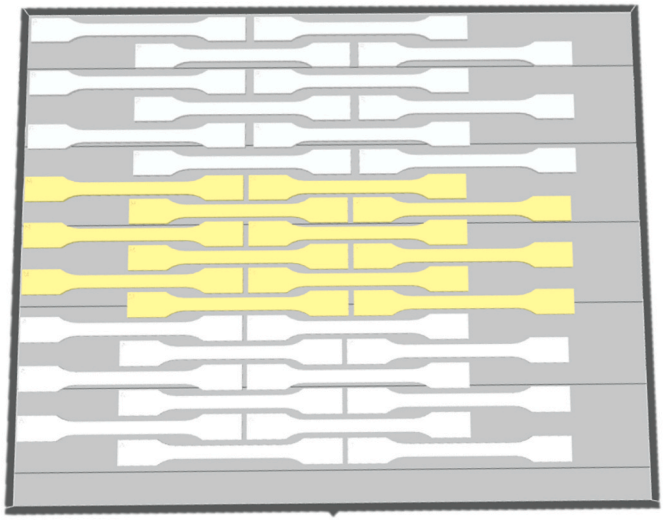

Fig. 1. Orientation of test specimens in GrabCAD Print software.

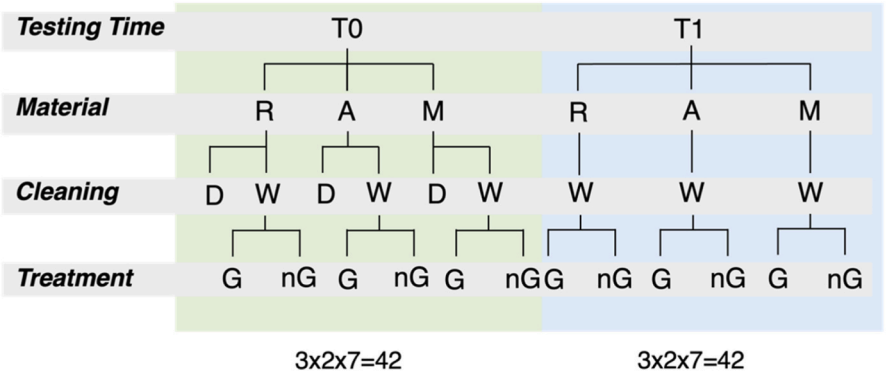

Testing Time
- T0 = within 48 hours from the printing;
- T1 = aging period of 30 days in a controlled environment.

Material
- R (RIGID) = VeroPureWhite;
- A (AGILUS) = Agilus30 White;
- M (MIXED) = Agilus30 White + VeroPureWhite (Shore A-60).

Cleaning
- Dry (D) = support removal in dry conditions;
- Water (W) = support removal with a waterjet station.

Treatment
- G = specimens soaked in a 15% glycerol solution after cleaning;
- nG = no treatment after cleaning.

Fig. 2. Schematic diagram of the experimental design of the study.

Fig. 3. Specimens undergoing aging in a controlled environment and intended for tensile tests after 30 days of aging.

Fig. 4. The Agilus30 White (A) specimen loaded in the Instron UTS machine during the tensile testing.

was removed from the specimens using the same soaking station with water. The specimens were tested within 48 h after the printing (T0) and after a period of natural aging in a controlled environment (T = 23 ± 1.8°C, UR = 38 ± 5%) of 60 days (T1), 90 days (T2) and 180 days (T3).

2.3. Tensile testing

We conducted a series of standard tensile tests on the specimens using the INSTRON 5966 machine (Instron, Norwood, USA) (10 kN load cell). A preload of 1N was applied to the specimens at a controlled rate of 2 mm/min. Following the preload, the specimens were subjected to primary mechanical testing at a constant rate of 50 mm/min. To avoid errors caused by the physical distortion occurring during the first part of traction, a static axial clip-on extensometer (Instron, Norwood, USA) was used and removed after reaching the preload value. Five specimens for each group of materials (R, A, M) and conditions [WT0: water-cleaned (W) parts tested within 48 h after printing (T0); GT0: parts treated with glycerol (G) and tested within 48 h after printing (T0); WT1: water-cleaned (W) parts tested after an aging period (T1); GT1: glycerol-treated (G) parts tested after an aging period (T1)] were tested (Fig. 4).

2.4. Shore hardness testing

The Shore A hardness tests were performed using a portable Affri 3001 Shore A Hardness Tester (Affri Inc., Varese, Italy). The instrument

Fig. 5. Hardness testing on the cuboid specimen using a Shore-A durometer.

has a capacity range from 0 to 100 with a tolerance of ±1. The reading of the value was taken according to the ISO 48–4:2018, for each cuboid specimen (Fig. 5). The measurements were performed on three faces of the cube, each representative of a different printing direction (XY, YZ, ZX).

2.5. Data evaluation and statistical methods

SPSS software, version 26.0 (SPSS Inc., Chicago, IL, United States) was used to perform a statistical analysis to compare the groups of specimens undergoing different post-printing processing and aging conditions. Specifically, a *t*-test (DoF = 8) was applied in order to determine whether there is a statistically significant difference between the means of groups.

During the analysis, a confidence level of 95% was adopted, meaning that the difference between the means of groups is considered statistically significant if the p-value < 0.05.

3. Results

3.1. Results of tensile tests

Sample comparisons of the obtained stress-strain curves of the three different materials are shown in Fig. 6. Mean tensile properties and corresponding standard deviations of the tested material types at different post-printing processing/aging conditions are reported in Table 2. A graphical illustration of the obtained mechanical data is given in Fig. 7: minimum (low value of the histogram), maximum (high value of the histogram), mean (dot) and standard deviations (bars) values are reported. Statistically significant differences for the various post-printing processing/aging conditions with the obtained p-values between groups are highlighted in bold in Table 2.

Regarding the specimens fabricated with Agilus30White (A type), the use of glycerol after the printing (GT0) has the effect of increasing the Young's modulus (E), decreasing the ultimate tensile strength (σ_u), and coherently decreasing the elongation at break (ε_u). The aging process (T1) on type A material has the effect of partially reach values of pre-treatment levels in the mechanical properties (E, σ_u, ε_u) induced by cleaning the parts using only water (W) or also adding glycerol (G).

In all the specimens fabricated with VeroPureWhite (R) the immediate post-printing processing with both water (WT0) and glycerol (GT0) reduces both E and σ_u, while ε_u is quite maintained except for the case of applying glycerol. In any case, under the effect of aging, the R material becomes more deformable (higher ε_u values) without no longer recovering the initial E and σ_u values. Indeed, all the obtained E and σ_u values after aging fell below the minimum level reported in the datasheet range (Fig. 7, Table 2).

Regarding the mixed specimens (M), the immediate post-printing processing with water (WT0) reduces E, σ_u and ε_u, while when using glycerol (GT0) the E tends to increase if compared with WT0 and both σ_u and ε_u still decrease. Under the effect of aging, the specimen treated with glycerol (GT1) showed an increase in both σ_u and ε_u, while E decreased. For the aged specimen cleaned only with water (WT1), all mechanical parameters (E, σ_u and ε_u) decreased.

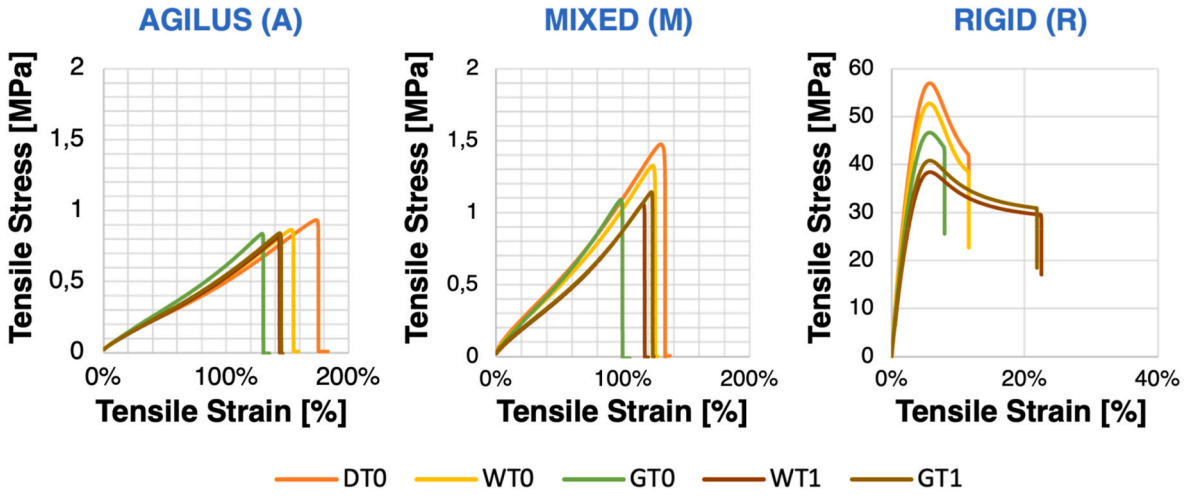

Fig. 6. Comparison of stress-strain curves obtained for the three material types (A, M, R) at different tested conditions. Every curve represents a single specimen considered representative for that material type. DT0: condition of dry cleaned (D) parts within 48 h after printing (T0); WT0: condition of water-cleaned (W) parts tested within 48 h after printing (T0); GT0: condition of parts treated with glycerol (G) and tested within 48 h after printing (T0); WT1: condition of water-cleaned (W) parts tested after aging period (T1); GT1: condition of glycerol-treated (G) parts tested after aging period (T1).

Table 2
The obtained mean tensile data (n = 5 for each mechanical property and each group) and corresponding standard deviations (E: modulus of elasticity, σ_u: tensile strength, ε_u: elongation at break). DT0: condition of dry cleaned (D) parts within 48 h after printing (T0); WT0: condition of water-cleaned (W) parts tested within 48 h after printing (T0); GT0: condition of parts treated with glycerol (G) and tested within 48 h after printing (T0); WT1: condition of water-cleaned (W) parts tested after aging period (T1); GT1: condition of glycerol-treated (G) parts tested after aging period (T1).

Material	Group	E (Mpa)		σ_u (Mpa)		ε_u (%)	
		Mean	SD	Mean	SD	Mean	SD
Agilus30White (A)	DT0	0.70	0.07	0.94	0.08	178.30	13.76
	WT0	0.83	0.08	0.87	0.06	157.31	11.81
	GT0	1.03	0.15	0.81	0.04	126.39	3.62
	WT1	0.78	0.09	0.84	0.03	140.76	3.13
	GT1	0.83	0.07	0.89	0.04	144.94	2.14
VeroPureWhite + Agilus30White (M)	DT0	1.72	0.10	1.60	0.08	134.87	4.40
	WT0	1.49	0.16	1.33	0.08	123.86	3.33
	GT0	1.53	0.12	1.05	0.07	100.34	2.94
	WT1	1.12	0.11	1.06	0.03	116.18	3.39
	GT1	1.19	0.09	1.14	0.02	122.30	1.28
VeroPureWhite (R)	DT0	2074.75	62.42	58.95	1.32	12.08	1.44
	WT0	1940.52	52.81	55.24	1.46	12.54	2.47
	GT0	1606.89	35.75	46.29	0.92	7.99	1.99
	WT1	1365.41	103.79	40.51	2.27	22.70	1.69
	GT1	1425.12	97.91	42.25	1.80	22.01	2.51

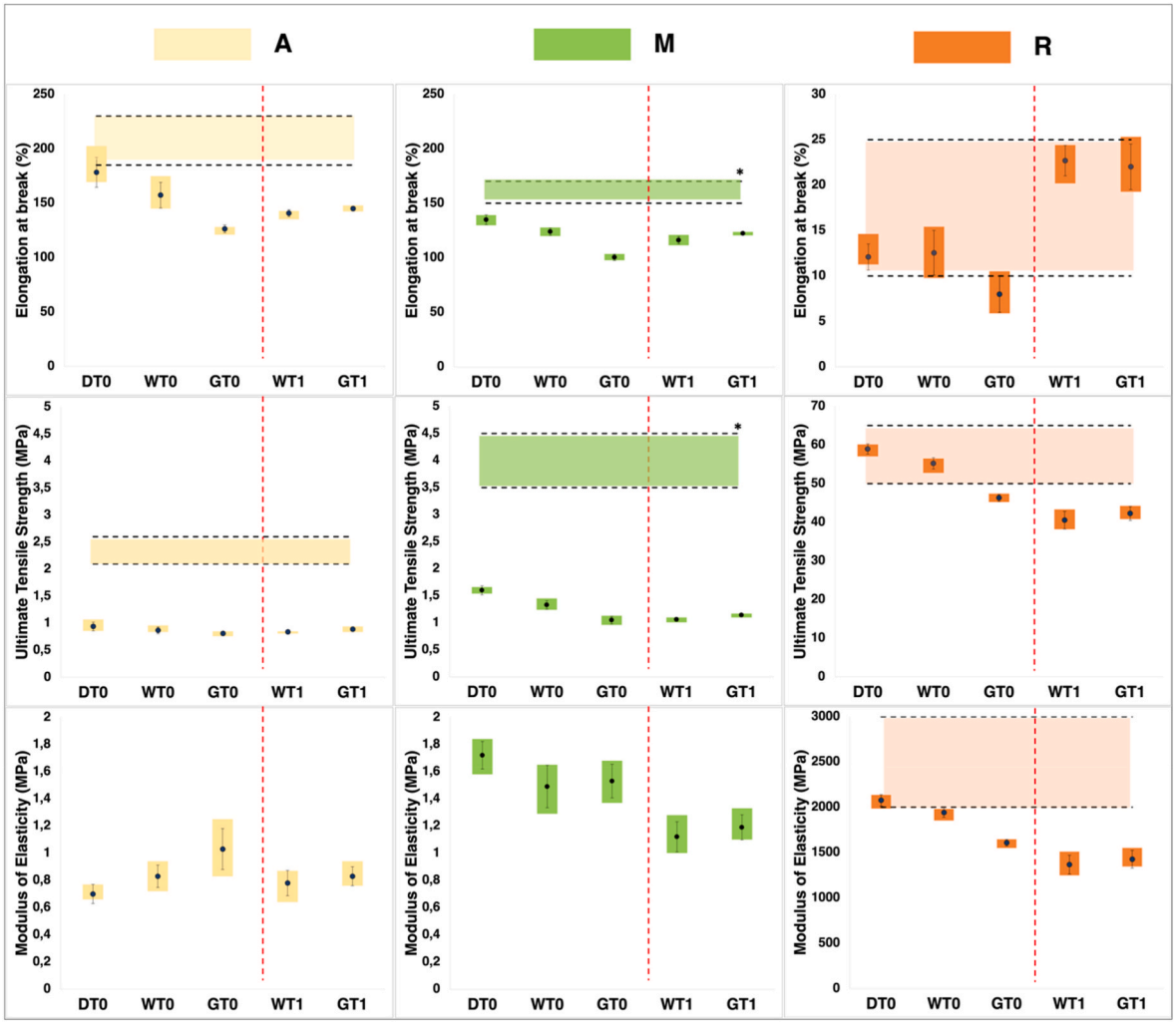

Fig. 7. Boxplots of the mechanical data of all tested materials (A, M, R). On the left side are represented the results of different post-printing processing (D, W, G), while on the right side the results after aging (T1). The horizontal band delimited by hatchings represents the reference values reported in the materials datasheet (Note: E values for A and M materials are lacking in the datasheet). *The only available datasheet values are referred to the mixture of Agilus30 Clear/Black and VeroFamily materials.

Table 3
The p-values obtained from the statistical *t*-test (E: modulus of elasticity, σ_u: tensile strength, ε_u: elongation at break) performed for the comparative analysis. In bold the values showing significant differences between the compared groups.

Material	Group	E (Mpa)	σ_u (Mpa)	ε_u (%)
Agilus30White (A)	DT0 vs. WT0	**0.012**	0.102	**0.016**
	WT0 vs. GT0	**0.016**	0.060	**0.000**
	WT0 vs. WT1	0.225	0.158	**0.008**
	GT0 vs. GT1	**0.016**	**0.007**	**0.000**
	WT1 vs. GT1	0.183	**0.025**	**0.020**
VeroPureWhite + Agilus30White (M)	DT0 vs. WT0	**0.012**	**0.000**	**0.001**
	WT0 vs. GT0	0.296	**0.000**	**0.000**
	WT0 vs. WT1	**0.001**	**0.000**	**0.003**
	GT0 vs. GT1	**0.001**	**0.015**	**0.000**
	WT1 vs. GT1	0.143	**0.001**	**0.003**
VeroPureWhite (R)	DT0 vs. WT0	**0.003**	**0.001**	0.362
	WT0 vs. GT0	**0.000**	**0.000**	**0.006**
	WT0 vs. WT1	**0.000**	**0.000**	**0.000**
	GT0 vs. GT1	**0.002**	**0.001**	**0.000**
	WT1 vs. GT1	0.188	0.109	0.311

In Table 3 the *p*-values obtained from the statistical analysis are reported and the statistically significant values between the different tested conditions are highlighted in bold.

3.2. Results of shore hardness tests

In Fig. 8 the results obtained from Shore measurements are reported. At T0 the measured values were clearly inferior to the ones set as printing input, except for the extreme values (Shore A30 and Shore A95) which were closer to the theoretical set values. Generally, the higher Shore A values were obtained for the XY face of the specimen, compared to those obtained for the YZ and XZ faces. This trend is maintained also after aging. Particularly, from T0 to T2 (90 days of aging) there was a decreasing trend in the measured hardness, while, at T3 (180 days of aging) there was a "recovery" of hardness which tends to approach the initial value (T0) (Fig. 8). Mean hardness values and corresponding standard deviations of the tested material types, at different face orientation and different aging times, are reported in Table 4.

4. Discussion

The study aimed to assess the mechanical properties of two frequently used PolyJet materials, i.e. rigid VeroPureWhite (R) and flexible Agilus30White (A), and a combination of them (M) to obtain a DM having an intermediate hardness (Shore A60).

The investigation encompassed the effects of both post-printing processing and aging on the mechanical properties (E, σ_u, ε_u) of the three types of material. The results collected in this study provided information on how these materials change their properties over time and after post-printing processing, giving valuable insights for the fabrication of advanced surgical simulators.

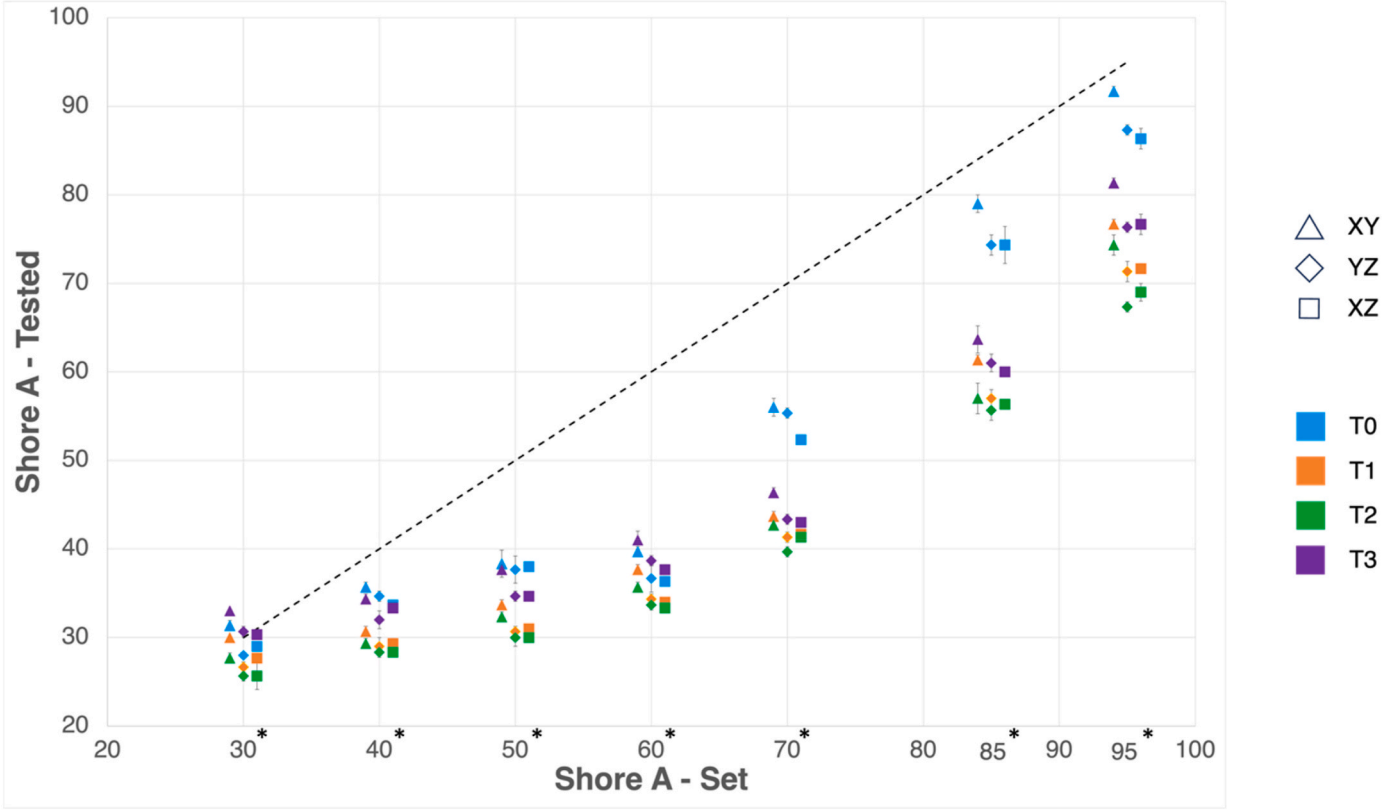

Fig. 8. Results for hardness tests, reported for different testing times (T0, T1, T2, T3) and testing faces (XY, YZ, XZ) of the cuboid specimens. On the X-axis is reported the Shore A set in GrabCAD Print software, while on the Y-axis the measured Shore A, within the range 0–100. The dashed line represents the theoretical linear relationship between the set Shore A value and the tested Shore A (i.e. the one obtained for the printed specimens). Values with asterisks represent the specific Shore values selected for testing within the range. T0: within 48 h after printing; T1: after 30 days of aging; T2: after 90 days of aging; T3: after 180 days of aging.

Table 4
Mean values and corresponding standard deviations obtained from the shore hardness test, divided by face orientation on printing tray and time of testing. T0: specimens tested after 48 h from the printing; T1: specimens tested after 30 days of aging period; T2: specimens tested after 90 days of aging period; T3: specimens tested after 180 days of aging period.

Shore A Set	Time	Shore A Tested					
		XY		YZ		XZ	
		Mean	SD	Mean	SD	Mean	SD
30	**T0**	31	1	28	0	29	0
	T1	30	0	27	1	28	1
	T2	28	1	26	1	26	2
	T3	33	0	31	1	30	1
40	**T0**	36	1	35	1	34	1
	T1	31	1	29	1	29	1
	T2	29	1	28	1	28	1
	T3	34	1	32	1	33	1
50	**T0**	38	1	38	2	38	0
	T1	34	1	31	1	31	0
	T2	32	1	30	1	30	0
	T3	38	1	35	1	35	1
60	**T0**	40	1	37	2	36	1
	T1	38	1	34	1	34	0
	T2	36	1	34	1	33	1
	T3	41	1	39	1	38	1
70	**T0**	56	1	55	1	52	1
	T1	44	1	41	1	42	1
	T2	43	1	40	1	41	1
	T3	46	1	43	1	38	1
85	**T0**	79	1	74	1	74	2
	T1	61	1	57	1	56	1
	T2	57	2	56	1	56	1
	T3	64	2	61	1	60	0
95	**T0**	92	1	87	1	86	1
	T1	77	1	71	1	72	1
	T2	74	1	67	1	69	1
	T3	81	1	76	1	77	1

In this study, a combination of printing parameters already suggested in the literature for the Polyjet materials was adopted. Particularly, previous studies reported that specimens should be placed with the critical load direction along the X-axis of the printer to achieve the best mechanical properties (Cazón et al., 2014), (Bass et al., 2016), (Wei et al., 2019). Moreover, Pugalendhi et al. (2020) reported that the specimens with a glossy finish show fewer peaks and valleys and better mechanical properties if compared to a matte finish. We also placed the specimens with their long axis along the printer X-axis, although when printing models for surgical simulators is quite hard to assure such an orientation, due to the complexity of the anatomical geometries.

About finishing, we used a matte finish, since for surgical simulators is advisable to have models with homogenous surfaces; indeed for complex geometries, as in the case of anatomical parts, it is not possible to achieve a homogenous glossy surfaces, therefore matte finishing is the only possible option. Moreover, a matte surface finish allows the printing of sharp edges, as the parts are completely covered in the support material, and this is essential to reproduce detailed anatomical structures in a surgical simulator.

Results of the tensile tests have shown that ε_u already at T0 (non-aged) for both A and M material are below the range declared in the datasheet, regardless of the type of post-printing process used.

This discrepancy could be due to the different tensile test standard and the unknown testing rate used to obtain the datasheet values.

Particularly the A samples dipped in glycerol after the printing (GT0) seem to have the lowest ε_u value. The same considerations can be made for M material, although the ε_u reduction is less evident due to a portion of rigid material inside the mixing. It must be specified that the obtained ε_u and σ_u values for M type are not strictly comparable to datasheet values since the manufaturer provides mechanical properties only for the combination of Agilus30 Clear or Black and VeroFamily materials.

Regarding ε_u, the R material is the only one for which all the measured values remain within the datasheet range, except for the case of samples dipped in glycerol solution which are just out of the lower boundary of this range.

Regarding E, the manufacturer does not provide a range in the datasheet for A and M materials. Conversely, for R material E values resulted lower than that declared in the datasheet for all testing conditions, apart from dry treatment (DT0). For A at T0, the glycerol samples (GT0) show the highest E value if compared to DT0, as glycerol tends to stiffen the material, acting as a sort of plasticizer, as suggested by the manufacturer. At T0, the R samples seem to have an opposite E trend under the effect of glycerol (GT0), i.e. to lose stiffness immediately after applying the glycerol, even if also ε_u and σ_u decrease. For M samples, E has a behaviour quite similar to that of the R samples, probably because the rigid part prevails on the flexible component inside the specimens.

Regarding σ_u, the obtained results for A and M materials are much lower than the minimum value of the range declared in the datasheet. Conversely, for R specimens were found σ_u values more consistent with the datasheet at T0, for both the dry (DT0) and the water-cleaned conditions (WT0) while, when dipping the part in glycerol (GT0), the σ_u value drops below the datasheet range.

Regarding R-type material, in this study we tested the VeroPure-White which is the latest update of the previous VeroWhitePlus polymer: the two materials have the same mechanical properties but the latest version (VeroPureWhite) is classified as a "Design Material" and has a better opacity. Several previous studies report differences in mechanical properties of VeroWhitePlus based on different orientations of the printed parts (Bass et al., 2016), (Mueller et al., 2015), (Barclift and Williams) but none of them consider the effect of different cleaning solutions or the use of glycerol after cleaning. Konigshofer et al. (Königshofer et al., 2021) tested the VeroPureWhite specimens cleaned with a water-jet station and after the conditioning in a controlled environment for 88 h. The tensile strength value obtained in the study (59 MPa), when using a printing orientation along XY axis and cleaning with water, is quite similar to the results found in this study (56 MPa). Regarding the modulus of elasticity (E), the value found in this study for VeroPureWhite (R) is 17% lower than the one found in their study, while for the elongation at break (ε_u) was found a 45% higher value, as if to demonstrate that the latest VeroPureWhite version is less rigid than the previous VeroWhitePlus version.

Interesting results are those obtained from tests on VeroPureWhite (R) samples after 30 days of aging. The obtained values were compared with the reference condition at T0 for each single post-printing processing (i.e. WT1 vs WT0, GT1 vs GT0). The ε_u showed an increase of 81% for those specimens only cleaned using water (WT1) and of 175% for those specimens treated with glycerol (GT1).

Consistently, E values showed a decrease of 30% for WT1 and 11% for GT1; for the ultimate tensile strength (σ_u), there was a decrease of 27% for WT1 and 9% for GT1. These results indicate that the R material loses its stiffness, thus becoming more deformable over time.

It must be also pointed out that few studies in the literature have focused on the effect of aging on the specimens of rigid Polyjet materials. The results of this study are consistent with those found by Bochnia (Bochnia, 2023), i.e. a decreasing trend for both σ_u and E. However, Bass et al. (2016) reported an increasing trend for σ_u and E, which became significant after 5 weeks of aging, while ε_u resulted in a decrease. Other groups focused their research on the aging effect on coloured materials of the Vero family (Matušú et al., 2021), (Vassilopoulos, 2022), (Costa et al., 2013), (Golhin et al., 2023). They report differences in the mechanical behavior between different coloured resins over time also depending on the printing direction, showing an overall reduction of the properties examined.

Regarding DMs, some groups focused their research on the development of predictive models for material mechanical behavior (Slesarenko and Rudykh, 2018). Nevertheless, none of them took into account the combination of Agilus30White and VeroPureWhite. Particularly in

M specimens, we observed a slight decrease of ε_u and σ_u after aging for those cleaned with water (WT1: 6% and −20%), while the ones treated with glycerol (GT1) showed an increase of 9% and 22%. Regarding E, the obtained values showed a decrease of 25% for WT1 and 20% for GT1. Therefore mixture M showed a mechanical behaviour similar to that of R material, suggesting that in the mixing, the rigid behaviour is predominant.

To date, no studies in the literature focused on the effect of aging on the rubber-like Agilus30White. Considering the possible application of this material for the fabrication of surgical simulation, especially for replicating soft tissues, it is important to understand how its mechanical behaviour changes over time. For this type of material, when cleaned only with water, was observed a decrease in the ability to deform after 30 days of aging; conversely, the subgroup of specimens treated with glycerol was able to deform more than the non-treated ones in the long term, as if they recover a little bit their original flexibility. Similarly, both for E (WT1: 6%) and σ_u (WT1: 4%), the water-cleaned specimens (WT1) show a slight decrease if compared to WT0, while the specimens treated with glycerol have a decrease for E (GT1: 19%) and an increase for σ_u (GT1: 10%). In this behaviour is interesting to note that the glycerol has a positive effect on the material in the long term, as it attempts to maintain the native mechanical properties of the material. This fact should be taken into account during the fabrication of surgical simulators, especially when the surgeons can not use the simulator within a short period of time after the printing.

The choice of post-printing treatments, such as the application of glycerol, has been shown to influence the mechanical properties of the 3D-printed parts, both immediately and in the long term. The resulting different mechanical behaviour based on post-printing processing methods emphasizes the importance of selecting the most appropriate treatment for a particular application.

The most interesting result obtained from the Shore hardness test is that the manufacturer overestimates the Shore value for the DMs obtained as a mixture of pure ones. Indeed, at T0, only for the Shore A30 and 95 we obtained values closer to those set in the printer. For all the other intermediate Shore A values (40, 50, 60, 70, 85), an underestimation of the hardness was observed. This findings was consistent with the experimental E values obtained for the M type material. Indeed, a relationship exists between stiffness (E) and hardness (Larson), therefore for Shore A60 the material should have E value of about 10 MPa, while we experimentally measured E values within the range of 0–2 MPa. All these observations could indicate that the settings imposed by GrabCAD for the mixtures actually overestimate the effective Shore A achievable for the printed part or that the printing process introduces some weaknesses when mixing different materials, thus resulting in mechanical performances lower than those expected.

Moreover, the aging until 60 days (T2) has the effect of further decrease the Shore value while after 180 days (T3) the Shore recovers till to approach the initial value. Generally, it can be observed that up to Shore A 60, where Agilus30White should predominate, the values obtained after aging differ less than the reference values at T0. On the contrary, for Shore values higher than A 60, in which the rigid material should predominate, the variation referred to T0 values is much more marked.

It is important to note that in the datasheets, the manufacturer does not state how long after printing the Shore hardness tests were carried out on the specimens. However, these findings show that an aging of 6 months (T3) tends to make all types of specimens stiffer than T1 and T2. This marked difference could be explained by a complete absorption of the water used during the cleaning of the parts after 6 months.

5. Limitations

It is important to acknowledge that this study has limitations. The effects of aging on mechanical properties (E, σ_u, ε_u) were examined over a relatively short period (i.e. after 30 days), and the behaviour over a longer time may differ. While for shore hardness tests we considered a longer period of aging, future research could explore more in detail the effects of the environmental conditions on the material properties.

An open question remains regarding whether and to what extent, the humidity of the support material may affect the properties of the printed parts. This could be achieved by including the measurement of the humidity in the polymer immediately after printing and after the removal of the support material. Moreover, after water cleaning, the change of the mechanical behaviour over time may also be related to the evaporation or the absorption of the water that may impact the resulting hardness. This aspect can be evaluated in future experiments by recording the masses of the specimens before and after the aging process. Additionally, microscopic tests could be performed to precisely evaluate the effects of water and glycerol on the microscopic structures forming the specimens, which could explain further the founded changes in the mechanical properties.

6. Conclusions

This study provides valuable data for selecting the appropriate material compositions and post-printing treatments to achieve the desired mechanical characteristics from Polyjet printing materials. Additionally, understanding the effects of aging on the material properties is crucial for designing long-lasting and reliable 3D-printed components of models intended for medical education and patient-specific surgical training. Within the conducted tensile tests, the results of this study demonstrate that different post-printing treatments influence the mechanical behaviour of the materials. Particularly, the treatment with glycerol immediately makes the rubber-like material (Agilus30White) more rigid, but then with aging the initial mechanical properties of flexibility/deformability tend to be restored.

Interestingly, aging has the effect of making more deformable the rigid VeroPureWhite. Another important aspect to consider during the fabrication of the surgical simulator deals with the real achievable Shore value of the DMs. When were tested various combinations of VeroPureWhite and Agilus30White, an important overestimation of the Shore values declared in the datasheet was found. Moreover, aging up to 90 days has the effect of further decrease the hardness, while after 180 days the hardness seems to recover.

CRediT authorship contribution statement

Nicolas Emiliani: Writing – original draft, Methodology, Conceptualization. **Rita Porcaro:** Writing – review & editing, Methodology, Data curation. **Gregorio Pisaneschi:** Supervision, Methodology, Data curation. **Barbara Bortolani:** Software, Data curation. **Fabrizio Ferretti:** Writing – review & editing, Validation. **Francesco Fontana:** Writing – review & editing, Methodology. **Giampaolo Campana:** Writing – review & editing, Supervision. **Maurizio Fiorini:** Supervision, Methodology. **Emanuela Marcelli:** Writing – review & editing, Supervision. **Laura Cercenelli:** Writing – review & editing, Supervision, Methodology, Conceptualization.

Declaration of competing interest

The authors declare that they have no known competing financial interests or personal relationships that could have appeared to influence the work reported in this paper.

Data availability

Data will be made available on request.

References

Aimar, A., Palermo, A., Innocenti, B., 2019. The role of 3D printing in medical applications: a state of the art. Journal of Healthcare Engineering 2019, 1–10. https://doi.org/10.1155/2019/5340616.

M. W. Barclift and C. B. Williams, 'EXAMINING VARIABILITY IN THE MECHANICAL PROPERTIES OF PARTS MANUFACTURED VIA POLYJET DIRECT 3D PRINTING'.

Bass, L., Meisel, N.A., Williams, C.B., 2016. Exploring variability of orientation and aging effects in material properties of multi-material jetting parts. RPJ 22 (5), 826–834. https://doi.org/10.1108/RPJ-11-2015-0169.

Bharucha, A.H., et al., 2023. Three-dimensional printing in modelling mitral valve interventions. Echo Res Pract 10 (1), 12. https://doi.org/10.1186/s44156-023-00024-x.

Blanco, D., Fernandez, P., Noriega, A., 2014. Nonisotropic experimental characterization of the relaxation modulus for PolyJet manufactured parts. J. Mater. Res. 29 (17), 1876–1882. https://doi.org/10.1557/jmr.2014.200.

Bochnia, J., 2023. A study of the mechanical properties of naturally aged photopolymers printed using the PJM technology. Materials 16 (1), 400. https://doi.org/10.3390/ma16010400.

Bustamante, S., Bose, S., Bishop, P., Klatte, R., Norris, F., 2014. Novel application of rapid prototyping for simulation of bronchoscopic anatomy. J. Cardiothorac. Vasc. Anesth. 28 (4), 1122–1125. https://doi.org/10.1053/j.jvca.2013.08.015.

Cazón, A., Morer, P., Matey, L., 2014. PolyJet technology for product prototyping: tensile strength and surface roughness properties. Proc. IME B J. Eng. Manufact. 228 (12), 1664–1675. https://doi.org/10.1177/0954405413518515.

Cheng, Y.-L., Huang, K.-C., 2020. Preparation and characterization of color photocurable resins for full-color material jetting additive manufacturing. Polymers 12 (3), 650. https://doi.org/10.3390/polym12030650.

Costa, C.A., Linzmaier, P.R., Pasquali, F.M., 2013. Rapid prototyping material degradation: a study of mechanical properties. IFAC Proc. Vol. 46 (24), 350–355. https://doi.org/10.3182/20130911-3-BR-3021.00118.

Dizon, J.R.C., Espera, A.H., Chen, Q., Advincula, R.C., 2018. Mechanical characterization of 3D-printed polymers. Addit. Manuf. 20, 44–67. https://doi.org/10.1016/j.addma.2017.12.002.

Erbano, B.O., et al., 2013. Rapid prototyping of three-dimensional biomodels as an adjuvant in the surgical planning for intracranial aneurysms. Acta Cir. Bras. 28 (11), 756–761. https://doi.org/10.1590/S0102-86502013001100002.

Gay, P., Blanco, D., Pelayo, F., Noriega, A., Fernández, P., 2015. Analysis of factors influencing the mechanical properties of flat PolyJet manufactured parts. Procedia Eng. 132, 70–77. https://doi.org/10.1016/j.proeng.2015.12.481.

Golhin, A.P., Srivastava, C., Strandlie, A., Sole, A.S., Grammatikos, S., 2023. Effects of accelerated aging on the appearance and mechanical performance of materials jetting products. Mater. Des. 228, 111863 https://doi.org/10.1016/j.matdes.2023.111863.

Grimaldo Ruiz, O., et al., 2022. Design and mechanical characterization using digital image correlation of soft tissue-mimicking polymers. Polymers 14 (13), 2639. https://doi.org/10.3390/polym14132639.

Hong, S.Y., et al., 2018. Experimental investigation of mechanical properties of UV-Curable 3D printing materials. Polymer 145, 88–94. https://doi.org/10.1016/j.polymer.2018.04.067.

Khan, I., Kelly, P., Singer, R., 2014. Prototyping of cerebral vasculature physical models. Surg. Neurol. Int. 5 (1), 11. https://doi.org/10.4103/2152-7806.125858.

Khoshkhoo, A., Carrano, A.L., Blersch, D.M., 2018. Effect of build orientation and part thickness on dimensional distortion in material jetting processes. RPJ 24 (9), 1563–1571. https://doi.org/10.1108/RPJ-10-2017-0210.

Kiraly, L., Tofeig, M., Jha, N.K., Talo, H., 2016. Three-dimensional printed prototypes refine the anatomy of post-modified Norwood-1 complex aortic arch obstruction and allow presurgical simulation of the repair. Interact. Cardiovasc. Thorac. Surg. 22 (2), 238–240. https://doi.org/10.1093/icvts/ivv320.

Komai, Y., et al., 2016. Patient-specific 3-dimensional printed kidney designed for "4D" surgical navigation: a novel aid to facilitate minimally invasive off-clamp partial nephrectomy in complex tumor cases. Urology 91, 226–233. https://doi.org/10.1016/j.urology.2015.11.060.

Königshofer, M., Stoiber, M., Unger, E., Grasl, C., Moscato, F., 2021. Mechanical and dimensional investigation of additive manufactured multimaterial parts. Front. Physiol. 9, 635736 https://doi.org/10.3389/fphy.2021.635736.

Kurenov, S.N., Ionita, C., Sammons, D., Demmy, T.L., 2015. Three-dimensional printing to facilitate anatomic study, device development, simulation, and planning in thoracic surgery. J. Thorac. Cardiovasc. Surg. 149 (4), 973–979.e1. https://doi.org/10.1016/j.jtcvs.2014.12.059.

Kusaka, M., et al., 2015. Initial experience with a tailor-made simulation and navigation program using a 3-D printer model of kidney transplantation surgery. Transplant. Proc. 47 (3), 596–599. https://doi.org/10.1016/j.transproceed.2014.12.045.

Langdon, C., et al., 2023. 3D printing as surgical planning and training in pediatric endoscopic skull base surgery - systematic review and practical example. Int. J. Pediatr. Otorhinolaryngol. 168, 111543 https://doi.org/10.1016/j.ijporl.2023.111543.

K. Larson, 'Can You Estimate Modulus from Durometer Hardness for Silicones?'.

Matušú, M., et al., 2021. The Effects of the Printing Direction and UV Artificial Degradation on the Mechanical Properties Using AM PolyJet Technology. ACM. https://doi.org/10.24132/acm.2021.649.

Molinari, G., et al., 2022. Assessment of a novel patient-specific 3D printed multi-material simulator for endoscopic sinus surgery. Front. Bioeng. Biotechnol. 10, 974021 https://doi.org/10.3389/fbioe.2022.974021.

Moore, J.P., Williams, C.B., 2015. Fatigue properties of parts printed by PolyJet material jetting. Rapid Prototyp. J. 21 (6), 675–685. https://doi.org/10.1108/RPJ-03-2014-0031.

Mueller, J., Shea, K., Daraio, C., 2015. Mechanical properties of parts fabricated with inkjet 3D printing through efficient experimental design. Mater. Des. 86, 902–912. https://doi.org/10.1016/j.matdes.2015.07.129.

Plastics, 2023. Determination of Tensile Properties. Part 4, Test Conditions for Isotropic and Orthotropic Fibre-Reinforced Plastic Composites. British Standards Institution, London.

Pugalendhi, A., Ranganathan, R., Chandrasekaran, M., 2020. Effect of process parameters on mechanical properties of VeroBlue material and their optimal selection in PolyJet technology. Int. J. Adv. Manuf. Technol. 108 (4), 1049–1059. https://doi.org/10.1007/s00170-019-04782-z.

Rubber, vulcanized or thermoplastic, 2018. Determination of hardness Indentation hardness by durometer method (Shore hardness). Definitive 1–15. First edition 2018-08.

Slesarenko, V., Rudykh, S., 2018. Towards mechanical characterization of soft digital materials for multimaterial 3D-printing. Int. J. Eng. Sci. 123, 62–72. https://doi.org/10.1016/j.ijengsci.2017.11.011.

Souzaki, R., et al., 2015. Three-dimensional liver model based on preoperative CT images as a tool to assist in surgical planning for hepatoblastoma in a child. Pediatr. Surg. Int. 31 (6), 593–596. https://doi.org/10.1007/s00383-015-3709-9.

Stansbury, J.W., Idacavage, M.J., 2016. 3D printing with polymers: challenges among expanding options and opportunities. Dent. Mater. 32 (1), 54–64. https://doi.org/10.1016/j.dental.2015.09.018.

Stratasys, 2016. Guide to Post-Printing Processes.

Sun, Z., Wong, Y.H., Yeong, C.H., 2023. Patient-specific 3D-printed low-cost models in medical education and clinical practice. Micromachines 14 (2), 464. https://doi.org/10.3390/mi14020464.

Suzuki, M., et al., 2022. Repetitive simulation training with novel 3D -printed sinus models for functional endoscopic sinus surgeries. Laryngoscope Investig Oto 7 (4), 943–954. https://doi.org/10.1002/lio2.873.

Tee, Y.L., Peng, C., Pille, P., Leary, M., Tran, P., 2020. PolyJet 3D printing of composite materials: experimental and modelling approach. JOM 72 (3), 1105–1117. https://doi.org/10.1007/s11837-020-04014-w.

Tyagi, S., Yadav, A., Deshmukh, S., 2022. Review on mechanical characterization of 3D printed parts created using material jetting process. Mater. Today: Proc. 51, 1012–1016. https://doi.org/10.1016/j.matpr.2021.07.073.

Valls-Esteve, A., et al., 2023. Advanced strategies for the fabrication of multi-material anatomical models of complex pediatric oncologic cases. Bioengineering 11 (1), 31. https://doi.org/10.3390/bioengineering11010031.

Vassilopoulos, A., 2022. Proceedings of the 20th European Conference on Composite Materials - Composites Meet Sustainability, vols. 1–6. https://doi.org/10.5075/EPFL-298799_978-2-9701614-0-0.

Vaz, V.M., Kumar, L., 2021. 3D printing as a promising tool in personalized medicine. AAPS PharmSciTech 22 (1), 49. https://doi.org/10.1208/s12249-020-01905-8.

Wake, N., Chandarana, H., Huang, W.C., Taneja, S.S., Rosenkrantz, A.B., 2016. Application of anatomically accurate, patient-specific 3D printed models from MRI data in urological oncology. Clin. Radiol. 71 (6), 610–614. https://doi.org/10.1016/j.crad.2016.02.012.

Wei, X., Bhardwaj, A., Shih, C.-C., Zeng, L., Tai, B., Pei, Z., 2019. Experimental investigation of stratasys J750 PolyJet printer: effects of orientation and layer thickness on mechanical properties. In: *Additive Manufacturing; Manufacturing Equipment and Systems; Bio and Sustainable Manufacturing*, Erie, Pennsylvania, USA, vol. 1. American Society of Mechanical Engineers, V001T01A021. https://doi.org/10.1115/MSEC2019-2717.

Wurm, G., Lehner, M., Tomancok, B., Kleiser, R., Nussbaumer, K., 2011. Cerebrovascular biomodeling for aneurysm surgery: simulation-based training by means of rapid prototyping technologies. Surg. Innovat. 18 (3), 294–306. https://doi.org/10.1177/1553350610395031.

Yang, D.H., Kang, J.-W., Kim, N., Song, J.-K., Lee, J.-W., Lim, T.-H., 2015. Myocardial 3-dimensional printing for septal myectomy guidance in a patient with obstructive hypertrophic cardiomyopathy. Circulation 132 (4), 300–301. https://doi.org/10.1161/CIRCULATIONAHA.115.015842.

Yap, Y.L., Wang, C., Sing, S.L., Dikshit, V., Yeong, W.Y., Wei, J., 2017. Material jetting additive manufacturing: an experimental study using designed metrological benchmarks. Precis. Eng. 50, 275–285. https://doi.org/10.1016/j.precisioneng.2017.05.015.

Yoo, S.-J., Spray, T., Austin, E.H., Yun, T.-J., Van Arsdell, G.S., 2017. Hands-on surgical training of congenital heart surgery using 3-dimensional print models. J. Thorac. Cardiovasc. Surg. 153 (6), 1530–1540. https://doi.org/10.1016/j.jtcvs.2016.12.054.

Zein, N.N., et al., 2013. Three-dimensional print of a liver for preoperative planning in living donor liver transplantation: three-Dimensional Printing. Liver Transplant. 19 (12), 1304–1310. https://doi.org/10.1002/lt.23729.

Agilus30 White Datasheet..

Datasheet Digital Materials..

Safety Datasheet Agilus30 White..

Safety Datasheet VeroPureWhite.

VeroFamily Datasheet..